Semnan University

Journal of Heat and Mass Transfer Research

Journal homepage: https://jhmtr.semnan.ac.ir

ISSN: 2383-3068

Research Article

Numerical Investigation on Transient Heat Transfer of Different Coolants in the Cooling Channel of a Thrust Chamber

Arash Haeri [a], Hamidreza Farshi Fasih [a]*, Roohollah Rafee [b]

[a] *Department of Aerospace Engineering, Faculty of New Science and Technologies, Semnan University, Semnan, Iran*

[b] *Faculty of Mechanical Engineering, Semnan University, Semnan, Iran*

ARTICLE INFO

Article history:

Received: 2026-01-29

Revised: 2026-03-05

Accepted: 2026-03-14

Keywords:

Cooling channel;

Wall temperature;

Coolant;

Heat flux;

Convective heat transfer.

ABSTRACT

Controlling the nozzle wall temperature using regenerative cooling is a highly effective approach in liquid rocket engines. The selection of coolant is critical to determining the cooling system's thermal performance. In this study, the transient and steady-state heat transfer characteristics of a regenerative cooling channel are numerically investigated using two benchmark coolants, water and Ethyl-alcohol, under different coolant mass flow rates. A two-dimensional axisymmetric conjugate heat transfer model is employed, in which the thrust chamber, cooling channel, and solid walls are fully coupled. For both coolants, the maximum gas-side wall temperature occurs upstream of the nozzle throat, and increasing the coolant mass flow rate significantly reduces both gas-side and coolant-side wall temperatures throughout the thrust chamber. Specifically, for water, the maximum wall temperature decreases from 657 K to 541 K as the mass flow rate increases from 0.5 to 1.5 kg/s, whereas for Ethyl-alcohol, it decreases from 957 K to 693 K. The time required to reach steady-state conditions for Ethyl-alcohol is approximately 1.8 times longer than that of water, while reducing the coolant mass flow rate from 1.0 to 0.5 kg/s nearly doubles the steady-state time. Moreover, the coolant mass flow rate strongly influences the peak heat flux and convective heat transfer coefficient upstream of the throat. Increasing the mass flow rate enhances heat transfer, so that at 1.5 kg/s the maximum heat flux is 21.0 MW/m^2 for water and 19.7 MW/m^2 for Ethyl-alcohol. Correspondingly, the convective heat transfer coefficient attains a peak value of approximately 7.8 kW/m^2·K near the throat and increases with increasing coolant mass flow rate. The results provide quantitative insights into transient thermal behavior and heat transfer mechanisms in regenerative cooling channels, offering helpful guidance for the thermal design and optimization of rocket engine thrust chambers.

© 2026 The Author(s). Journal of Heat and Mass Transfer Research published by Semnan University Press.
This is an open access article under the CC-BY-NC 4.0 license. (https://creativecommons.org/licenses/by-nc/4.0/)

1. Introduction

Accurate prediction of heat transfer characteristics is essential in the design of liquid-propellant rocket engines, particularly to ensure structural integrity, reusability, and long-term performance. The large temperature gradient between the high-temperature combustion gases and the nozzle wall generates intense heat fluxes, leading to elevated wall temperatures. Consequently, effective thermal management strategies are required to prevent material failure and extend the operational lifetime of the

* **Corresponding author.**
E-mail address: *farshifasih@semnan.ac.ir*

Cite this article as:
Haeri, A., Farshi Fasih, H. and Rafee, R., 2026. Numerical Investigation on Transient Heat Transfer of Different Coolants in the Cooling Channel of a Thrust Chamber. *Journal of Heat and Mass Transfer Research*, 13(2), pp. 207-218.
https://doi.org/10.22075/JHMTR.2026.40123.1914

thrust chamber. Among various thermal management techniques, regenerative cooling is widely recognized as one of the most effective approaches for high-pressure and high-temperature rocket engines. In this method, the propellant is circulated through cooling channels embedded in the chamber wall before entering the injector, thereby absorbing heat from the hot gas while simultaneously preheating the propellant. The selection of coolant and the cooling channel geometry are the most crucial parameters in achieving an optimal cooling strategy for liquid rocket engines. However, the design process requires balancing competing factors, including thrust chamber mass, thermal and mechanical loads resistance, and the power needed to circulate the coolant.

The thermal performance of regenerative cooling systems is strongly dependent on coolant properties and cooling channel geometry. Previous studies have investigated a wide range of coolants, including kerosene, cryogenic hydrogen and oxygen, liquid methane and nitrogen, supercritical CO_2, and hydrogen peroxide [1-4]. These investigations primarily focused on steady-state behavior, channel geometry optimization, and enhancement techniques such as ribbed or spiral channels. Heldens et al. [5] took initial steps to address the limited availability of data in the literature concerning the thermophysical properties of methane, specifically, high inlet temperatures and one-sided heat loads. The operating conditions involve mass flow rates, pressure, and inlet temperature of 15 g/s, 3 MPa, and 400 K, respectively. The one-sided heating significantly alters the flow field development. This phenomenon raises the heat transfer coefficient toward the cooling channel downstream. Kim et al. [6] presented an effective conjugate heat transfer and hydraulic model for kerosene in designing a regenerative cooling system. This model can incorporate key regenerative cooling parameters, such as channel geometry variations along the thrust chamber wall. It also reproduces the empirical relationship of coolant temperature increase and pressure loss on the mixture ratio. To enhance the thermal performance, Shanmugam et al. [7] investigated the influence of arc-shaped ribs on the heat transfer characteristics of a regenerative cooling channel employing supercritical hydrogen. The results indicated that the introduction of ribs markedly improved the coolant's heat capacity near the wall and effectively eliminated the peak wall temperature. Nasser et al. [8] have studied the thermophysical properties of LNG and determined the roughness characteristics needed to enhance cooling performance while maintaining an appropriate pressure drop. According to the results, the critical pressure is highly susceptible to hydrocarbon compounds. In critical transient processes and hydrocarbon compounds, different configurations of wall surface roughness affect the cooling characteristics and pressure drop. Engblom et al. [9] introduced a solver for modeling a cooling channel with water coolant and two-phase, low-velocity, and turbulent conditions. They concluded that this model, with high accuracy, could be utilized for predicting heat load in high-speed water-cooled flows.

Cooling channel geometry is another critical parameter in the optimal performance of a regenerative cooling system. The improved performance of the regenerative cooling channel is attributed to changes in aspect ratio, spiraling the channel along the thrust chamber, and placing various ribs with different arrangements [10-13]. Zhou et al. [14] investigated the influence of channel parameters and hydrogen peroxide coolant on regenerative cooling embedded in the thrust chamber. Reducing the inner wall thickness results in an increases the coolant outlet temperature and decrease in wall temperature. Moreover, increasing the height increases the internal wall temperature, slightly decreases the coolant temperature, and reduces the coolant pressure. Furthermore, increasing the width decreases the overall wall temperature. Junjie et al. [15] developed a model to assess the heat transfer parameters of a thrust chamber equipped with regenerative cooling spiral channels. The outcomes show that under the identical boundary conditions and channel geometry, the spiral channel significantly reduces the maximum inner wall temperature compared to that of the straight channel. Zhang et al. [16] proposed a novel ribbed channel structure to improve the heat dissipation capacity of cooling channels. Their results demonstrated that V-shaped ribs intensify secondary flow disturbances, thereby increasing heat transfer within the channels and ultimately reducing the wall temperature.

Furthermore, despite extensive research on regenerative cooling, detailed comparative studies addressing transient heat transfer behavior, the direct calculation of convective heat transfer coefficients, and the influence of coolant mass flow rate using benchmark fluids remain limited. In particular, transient thermal responses during engine start-up have received significantly less attention, despite their critical importance for structural safety. To address these gaps, the present study employs water and Ethyl-alcohol as benchmark cooling fluids to investigate heat transfer mechanisms in a regenerative cooling channel systematically.

Although these fluids are not representative of actual rocket propellants, their well-characterized thermophysical properties enable a precise and controlled assessment of transient and steady-state heat transfer behavior. The insights obtained from this comparative analysis provide transferable knowledge that supports the understanding of regenerative cooling physics and informs the selection and optimization of practical propellant-coolants in real rocket engine applications.

2. Methodology

2.1. Geometry and Boundary Conditions

In regenerative cooling, coolant is injected with a specific mass flow rate from the nozzle end into the cooling channel, flowing in the opposite direction to the hot gas stream. In this study, the thrust chamber profile and the geometry of the Marchi cooling channel are used [17]. Fig. 1 shows a schematic of the thrust chamber, and Table 1 provides their geometric specifications.

Table 1. Geometric of the thrust chamber and cooling channel, and characteristics of the hot gas flow and coolant

Thrust chamber and cooling channel	r_{ch} (m)	r_{th} (m)	ε	L_{ch} (m)	L_{no} (m)	z (mm)	t (mm)
	0.3	0.1	9	0.1	0.4	5	2
Hot gas flow	T_{in} (K)	P_{in} (bar)	T_{ex} (K)	P_{ex} (bar)	C_P (kJ/kg.K)	λ (W/m.K)	μ (kg/m.s)
	3424	20	1900	0.34	3.242	polynomial	sutherland
Coolant per channel	$\dot{m}$ (kg/s)	T_{in} (K)					
	0.5 – 1.5	300					

The variations in nozzle radius along the chamber length are calculated as follows:

$$r = r_{th} + \frac{r_{ch} - r_{th}}{2}\left\{1 + \cos\left[2\pi \frac{x - L_{ch}}{L_{no}}\right]\right\} \quad (x \geq L_{ch}) \quad (1)$$

The thrust chamber's inner wall is made of copper with λ=387.6 W/m.K and C_p=381 J/kg.K. It has high thermal conductivity and effectively dissipates heat. This prevents the formation of localized hot spots and promotes an uniform temperature distribution along the inner wall. [7]. Two cooling fluids, water and Ethyl-alcohol (C_2H_5OH), are selected for regenerative cooling. The characteristics of the hot gas and the coolant are presented in Table 1.

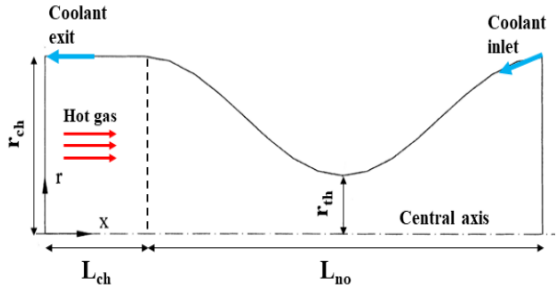

Fig. 1. Schematic of thrust chamber

2.2. Numerical Simulation and Validation

Generally, heat transfer in a combustion chamber employing regenerative cooling involves convective heat transfer between the hot gas and the inner wall, as well as between the coolant and the outer wall. This study considers the heat transfer model between the coolant and the nozzle wall, which is coupled [18]. The present modeling is axisymmetric, and the changes in cooling channel parameters are investigated along the horizontal axis of the thrust chamber. The calculation domain consists of two parts: the thrust chamber and the cooling channel, each meshed independently. Fig. 2 illustrates the structured grid of the solution domain. As can be seen, the mesh is denser near the wall and the cooling channel. To accurately resolve the thin boundary layers, the first grid height is selected to keep the dimensionless wall distance (y^+) within the range 1 to 4.

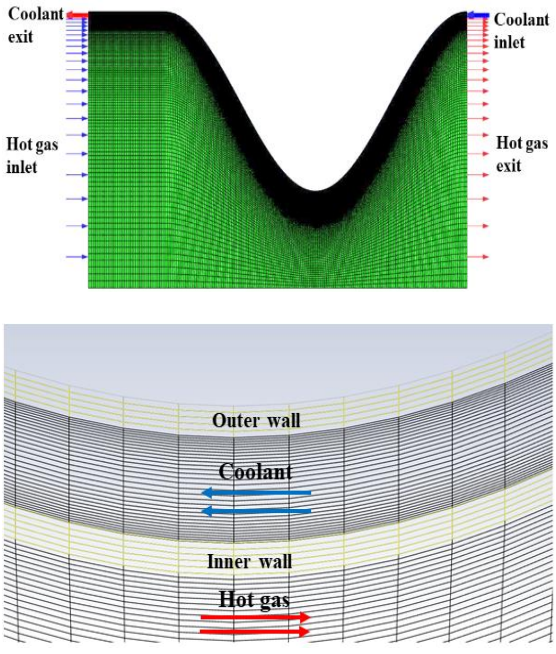

Fig. 2. Numerical domain grid

The software ANSYS Fluent 2022 R2 has been used to solve the conservation equations. The ideal gas equation of state and the incompressible liquid model are utilized for the hot gas and the coolant, respectively. Also, the Polynomial and Sutherland models are selected for the hot gas's thermal conductivity and viscosity, respectively. The ideal gas equation of state and conservation equations for energy, momentum, and mass are defined as follows [4]:

$$\frac{\partial \rho}{\partial t}+\frac{\partial}{\partial x_j}\left(\rho u_j\right)=0 \tag{2}$$

$$\frac{\partial}{\partial t}\left(\rho u_i\right)+\frac{\partial}{\partial x_j}\left(\rho u_j u_i\right)=-\frac{\partial P}{\partial x_i}+\frac{\partial \tau_{ij}}{\partial x_j} \tag{3}$$

$$\tau_{ij}=\left(\mu+\mu_t\right)\left(\frac{\partial u_i}{\partial x_j}+\frac{\partial u_j}{\partial x_i}-\frac{2}{3}\frac{\partial u_k}{\partial x_k}\delta_{ij}\right) \tag{4}$$

$$\frac{\partial}{\partial t}(\rho E)+\frac{\partial}{\partial x_i}\left(u_i(\rho E+P)\right)=\frac{\partial}{\partial x_j}\left[\left(\lambda+\frac{c_p \mu_t}{\mathrm{Pr}_t}\right)\frac{\partial T}{\partial x_j}+u_i\left(\tau_{ij}\right)_{eff}\right]+S_h \tag{5}$$

$$P=\rho R T \tag{6}$$

Considering the velocity components are zero in the solid region, the energy equation is used as follows:

$$\frac{\partial}{\partial t}(\rho H)+\frac{\partial}{\partial x_i}\left[u_i(\rho H)\right]=\frac{\partial}{\partial x_j}\left[\lambda\frac{\partial T}{\partial x_i}\right]+S_h \tag{7}$$

In the present study, the SST k-ω turbulence model is employed according to the following equations. This model has higher accuracy in solving the turbulent kinetic energy values near the walls. It also has strong performance in capturing turbulence with low Reynolds number in heat and mass transfer processes near the walls with variations in the thermophysical properties of the flow [19, 20].

$$\frac{\partial}{\partial t}(\rho k)+\frac{\partial}{\partial x_i}(\rho u_i k)=\frac{\partial}{\partial x_i}\left[\Gamma_k\frac{\partial k}{\partial x_i}\right]+G_k-Y_k \tag{8}$$

$$\frac{\partial}{\partial t}(\rho \omega)+\frac{\partial}{\partial x_i}(\rho u_i \omega)=\frac{\partial}{\partial x_j}\left[\Gamma_\omega\frac{\partial \omega}{\partial x_j}\right]+G_\omega-Y_\omega+D_\omega \tag{9}$$

where Γ_ω and Γ_k are the diffusivity of ω and k, G_ω and G_k are the generation of ω and k, and Y_ω and Y_k are the turbulence production due to diffusion. The boundary conditions for the inlet and outlet of the cooling channel are set as the mass-flow-inlet and out-flow, respectively. Moreover, the boundary conditions for the inlet and outlet of the thrust chamber are set as the pressure-inlet and pressure-outlet, respectively. Considering the incompressibility of the coolant and hot gas flow, a pressure-based model is used in the solver section. Also, a SIMPLEC approach is selected for velocity-pressure coupling. The convective term and viscous term are evaluated by the second-order upwind and central differencing, respectively. Solution convergence is evaluated using a residual criterion of 10^{-5}.

The following correlation is adopted to predict the Nusselt number with turbulent flow on thermal systems including cooling channels, in which all fluid physical properties are estimated at the mean bulk temperature [7]. This correlation is valid for the ranges $2300 \le \mathrm{Re} \le 10^7$ and $0.5 \le \mathrm{Pr} \le 120$.

$$\mathrm{Re}=\frac{GD_h}{\mu} \tag{10}$$

$$\mathrm{Pr}=\frac{\mu C_p}{\lambda} \tag{11}$$

$$Nu=0.023\,\mathrm{Re}^{0.8}\,\mathrm{Pr}^{0.4} \tag{12}$$

where Re and Pr are Reynolds and Prandtl number. Also, G is the mass flow rate per unit cross-sectional area, D_h is the hyadraulic diameter, μ is the viscosity, λ is the thermal conductivity, and C_p is the specific heat capacity of coolant.

In regenerative cooling studies for liquid rocket engines, the Bartz correlation calculates the convective heat transfer coefficient, requiring specific assumptions and approximations [21, 22]. However, the convective heat transfer coefficient between the hot gas and the gas-side wall is calculated directly using the heat flux and temperature difference as [12, 23]:

$$h=\frac{q}{\left(T_{wg}-T_{bg}\right)} \tag{13}$$

where q is the heat flux, T_{wg} is the gas-side wall temperature, and T_{bg} is the bulk gas temperature. The T_{bg} is defined as the mass-averaged temperature across each axial cross-section of the thrust chamber and is directly extracted from the numerical solution. An adiabatic condition is imposed on the outer wall of the cooling channel.

To examine the grid independence of the numerical results, the pressure distribution along the central axis of the thrust chamber is evaluated using different grid resolutions. Fig. 3 presents the pressure variation along the central axis as a function of the chamber length. Based on these results, a grid containing 11025 cells is selected for the final simulations. The results obtained from modeling the behavior of hot gas in the isentropic state have been validated with the research of [24]. Fig. 4 compares the static pressure at the upper wall, showing a 7% RMSE

(Root Mean Square Error) between the experimental data and the numerical results.

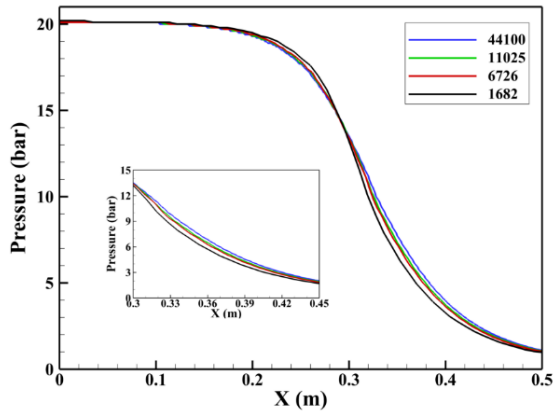

Fig. 3. Pressure distribution along the central axis of the thrust chamber for different grids

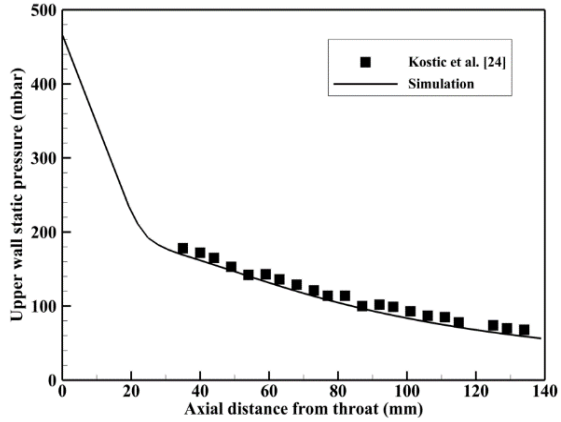

Fig. 4. Comparison of experimental data and modeling results

3. Results and Discussion

In this section, the Mach number and temperature of the hot gas flow are assessed under steady-state conditions. Then, the heat transfer characteristics of the regenerative cooling channel along the thrust chamber, including T_{wg}, T_{wc}, T_{cool} and heat flux are presented for different coolant mass flow rate in a steady-state condition. Additionally, the study investigates the transient thermal response of the thrust chamber wall for different coolant mass flow rate. Moreover, a primary objective of the study is to directly measure the convective heat transfer coefficient in the engine. By calculating the convective heat transfer coefficient, practical suggestions can be made for the design and optimization of the nozzle wall and cooling channel, as well as for extending the nozzle's lifespan. Therefore, changes in the convective heat transfer coefficient along the thrust chamber are among the other results of the present study.

3.1. Flow Field of Thrust Chamber

The Mach number and temperature values are averaged at different sections of the thrust chamber, and their variations along the longitudinal axis are presented in Fig. 5. As expected, the temperature and Mach number in the combustion chamber are approximately constant and equal to 3400 K and 0.1, respectively. In the converging section, the temperature and Mach number begin to decrease and increase, respectively. In the diverging section, the decrease in temperature and increase in Mach number continue at a higher rate, reaching 2150 K and 2.6, respectively, at the nozzle exit. A similar behavior of Mach number and temperature versus thrust chamber length has been observed in [25, 26].

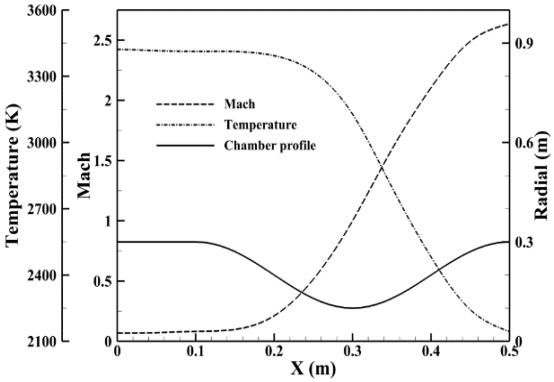

Fig. 5. The axial distribution of Mach and temperature in the thrust chamber

3.2. Distribution of Wall Temperature in Steady State

Fig. 6 depicts the variations of T_{wg} along the steady-state thrust chamber for two coolants, water and Ethyl-alcohol, and different mass flow rate. As the coolant enters the nozzle (x=0.5), T_{wg} has its minimum value at the nozzle end. The T_{wg} increases along the nozzle's divergent section from x=0.5 to x=0.3. T_{wg} reaches its maximum value upstream of the throat (x=0.29). This phenomenon is due to the q, heat transfer rate, and the effect of Dean vortices in the curved cooling channels [4, 18]. Following, a decreasing trend is observed from x=0.29 to x=0.12. Since the T_{cool} increases along the cooling channel, and the hot gas temperature also increases from the diverging to the converging section. It is expected that T_{wg} is higher at the converging of the nozzle compared to the nozzle end. Furthermore, because of the sudden change in the cooling channel geometry at x=0.12, vortices are generated in the cooling channel. This phenomenon increases the heat transfer of the coolant, resulting in a sectional drop in T_{wg} [27]. Due to the low velocity of the hot gas inside the

combustion chamber, the T_{wg} increases from x=0.12 to x=0, reaching a temperature approximately equal to the maximum value at the throat. A similar trend in the T_{wg} changes along the thrust chamber length has been reported in the studies by [14, 28]. The results also indicate that as the coolant mass flow rate increases from 0.5 to 1.5 kg/s, T_{wg} significantly decreases. The temperature variations of the inner wall are similar for both Ethyl-alcohol and water. However, since the specific heat capacity of Ethyl-alcohol is lower than that of water, Ethyl-alcohol has less cooling potential than water.

Table 2 presents a comparison of T_{wg} for water and Ethyl-alcohol, at three sections of the thrust chamber: the nozzle's diverging end (x=0.50), upstream of the throat (x=0.29), and the nozzle's converging start (x=1.2), and for three mass flow rate. The comparison of values shows that for each constant mass flow rate, the greatest difference of T_{wg} between two coolants occurs at x=0.29, x=0.12, and x=0.50, respectively. For instance, in $\dot{m} = 1\ kg/s$, the difference of T_{wg} between the two coolants is 197, 97, and 9 K in these three sections, respectively. Also, at a constant section, the difference of T_{wg} follows between two coolants with an increasing trend and a decrease in the mass flow rate. For instance, at x=0.29, the difference of T_{wg} between the two coolants is 152, 197, and 300 K for the three mass flow rate, respectively.

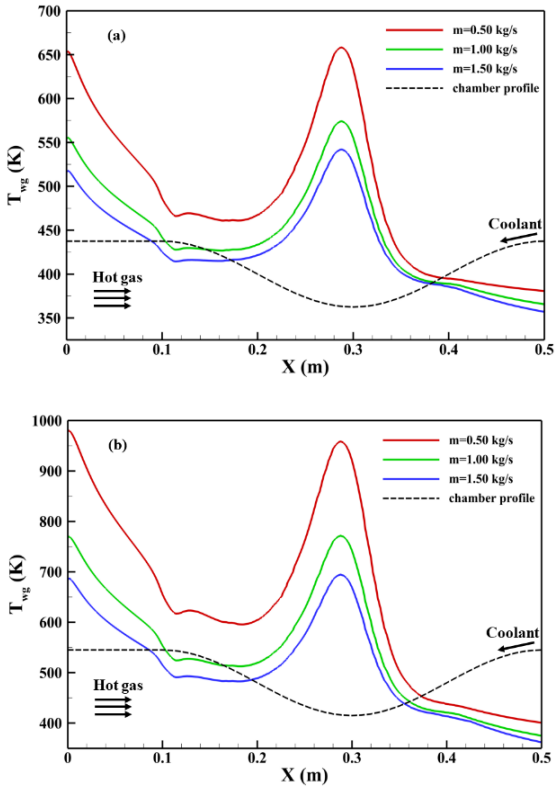

Fig. 6. Distribution of gas-side wall temperature: (a) water, (b) Ethyl-alcohol

Table 2. Comparison of gas-side wall temperature for two coolants

		x=0.12 m	x=0.29 m	x=0.50 m
T_{wg} (K) water	$\dot{m} = 1.5\ kg/s$	415	541	357
	$\dot{m} = 1\ kg/s$	429	573	366
	$\dot{m} = 0.5\ kg/s$	467	657	381
T_{wg} (K) Ethyl-alcohol	$\dot{m} = 1.5\ kg/s$	492	693	362
	$\dot{m} = 1\ kg/s$	526	770	375
	$\dot{m} = 0.5\ kg/s$	619	957	401

Fig. 7 illustrates T_{wg} and T_{wc} along the thrust chamber at coolant mass flow rate of 0.5 and 1.5 kg/s. Throughout the thrust chamber, the trends of T_{wc} and T_{wg} are similar, and the T_{wc} is lower than the T_{wg}. A similar behavior of T_{wg} and T_{wc} variations has been observed in the research of [15, 29]. Given the melting point of copper (1356 Kelvin) and the maximum inner wall temperature for water and Ethyl-alcohol (650 and 970 Kelvin, respectively), it can be concluded that the thrust chamber wall will function normally [30].

Table 3 presents the values of the (T_{wg}-T_{wc}) for two coolants at three sections (x=0.12, x=0.29, x=0.50) and for three mass flow rate. Comparing the results indicates that the highest temperature difference occurs upstream of the throat (x=0.29) for both coolants and at each mass flow rate. Also, this temperature difference decreases for each coolant and at x=0.29, as the mass flow rate decreases.

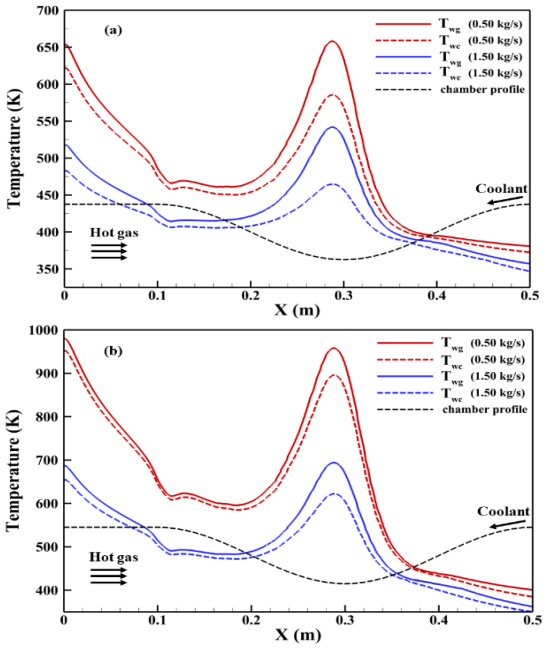

Fig. 7. Distribution of gas-side wall and coolant-side wall temperature: (a) water, (b) Ethyl-alcohol

Table 3. Comparison of the difference in gas-side and coolant-side wall temperature for two coolants

		x=0.12 m	x=0.29 m	x=0.50 m
T_{wg} - T_{wc} water	$\dot{m} = 1.5\ kg/s$	8	77	10
	$\dot{m} = 1\ kg/s$	9	75	7
	$\dot{m} = 0.5\ kg/s$	9	72	8
T_{wg} - T_{wc} Ethyl-alcohol	$\dot{m} = 1.5\ kg/s$	9	71	12
	$\dot{m} = 1\ kg/s$	9	68	12
	$\dot{m} = 0.5\ kg/s$	9	62	16

3.3. Distribution of Wall Temperature in Transient

The transient state is considered from the start-up of the engine until it reaches the steady state. Fig. 8 depicts the variations of T_{wg} along the thrust chamber for water and Ethyl-alcohol until reaching the steady state, and $\dot{m} = 0.5, 0.75, 1.0\ kg/s$. As the engine starts, the coolant enters the cooling channel from the divergent end and traverses the entire cooling channel to reach the beginning of the thrust chamber. Therefore, as can be seen, up to 0.5 seconds for water and 1 second for Ethyl-alcohol, only the divergent part of the nozzle (x=0.34 to 0.5) is affected by cooling, and its wall temperature is lower than that of the other parts. Subsequently, up to 1 second for water and 2 seconds for Ethyl-alcohol, the entire nozzle (x=0.12 to 0.5) is subjected to cooling, and the nozzle wall temperature is lower than the combustion chamber wall temperature.

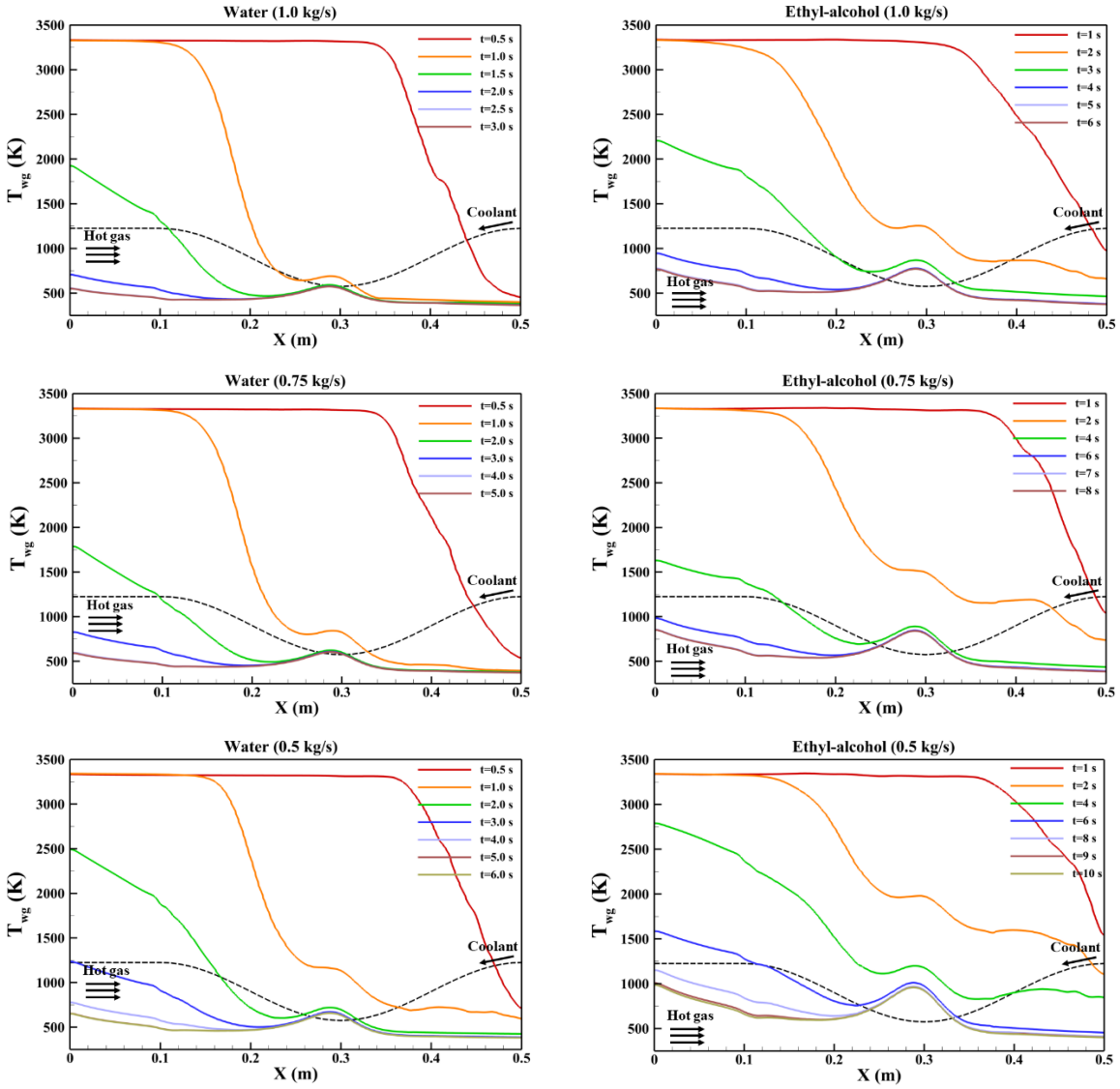

Fig. 8. Distribution of gas-side wall temperature in transient: (left) water, (right) Ethyl-alcohol

After 1 second for water and 2 seconds for Ethyl-alcohol, the entire thrust chamber experiences the regenerative cooling, and Twg gradually decreases. This process continues until the T_{wg} changes become negligible and reach a steady state.

Table 4 presents the two coolants' steady-state time of gas-side wall temperature. According to the results, decreasing the mass flow rate significantly increases the steady state time. Specifically, when the mass flow rate is halved from 1 to 0.5 kg/s, the steady state time of water doubles, rising by a factor of 1.8 for Ethyl-alcohol. Also, on average, the steady state time of Ethyl-alcohol is approximately 1.85 times that of water.

Table 4. Comparison of reaching time to steady-state for two coolants

	$\dot{m} = 1.0$ kg/s	$\dot{m} = 0.75$ kg/s	$\dot{m} = 0.5$ kg/s
water	2.5 s	4 s	5 s
Ethyl-alcohol	5 s	7 s	9 s

3.4. Distribution of Convective Heat Transfer Coefficient

According to obtaining of convective heat transfer based on equation (13), the heat flux of the hot gas must first be determined. Fig. 9 depicts the heat flux variations along the thrust chamber for different coolant mass flow rate. The heat flux shows a decreasing trend along the combustion chamber due to the development of the boundary layer along the hot gas wall. As the turbulent boundary layer thickness increases along the chamber, the heat flux gradually decreases [31]. From the beginning of the converging nozzle (x=0.12), the heat flux increases and reaches its maximum value upstream of the throat (x=0.28). In the diverging nozzle, due to the hot gas flow's expansion and the boundary layer's small thickness, the heat flux decreases until it reaches its minimum value at the end of the nozzle. A similar trend of heat flux variations along the chamber length has been reported in the investigations [32-34]. The coolant mass flow rate is effective on the critical heat flux upstream of the throat, such that by increasing mass flow rate, the critical heat flux also increases [1]. For mass flow rate of 0.5, 1.0, and 1.5 kg/s, the maximum heat flux is 19.8, 20.7, and 21.0 MW/m^2 for water and 17.1, 18.9, and 19.7 MW/m^2 for Ethyl-alcohol, respectively. On average, the maximum heat flux of water is 1.9 times higher than that of Ethyl-alcohol for different mass flow rate.

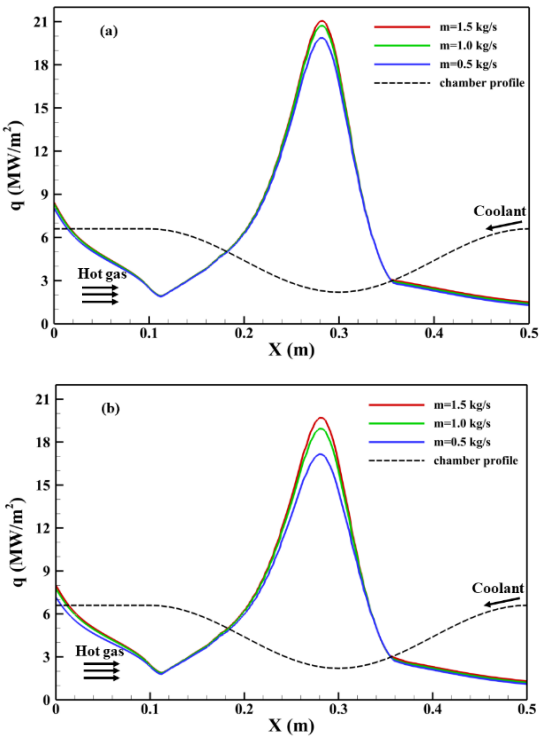

Fig. 9. Distribution of heat flux: (a) water, (b) Ethyl-alcohol

Now, considering Figs. 5, 6, and 9, as well as equation (13), the convctive heat transfer coefficient can be directly determined. Fig. 10 illustrates the distribution of the convctive heat transfer coefficient as a function of nozzle length for different coolant mass flow rate. The convctive heat transfer coefficient reaches its maximum value of approximately 7.8, upstream of the throat (x=0.28), and decreases on both sides of the nozzle, reaching 0.84 in the converging section and 0.8 in the diverging section. Similar behavior of the convctive heat transfer coefficient has been observed in the research of [21, 35]. Only upstream of the throat, the coolant mass flow rate affects the wall heat transfer coefficient. As the coolant mass flow rate increases, the convctive heat transfer coefficient of the wall also increases [5]. On average, the convctive heat transfer coefficient for water is 0.12 higher than that for Ethyl-alcohol, upstream of the throat, and all mass flow rate.

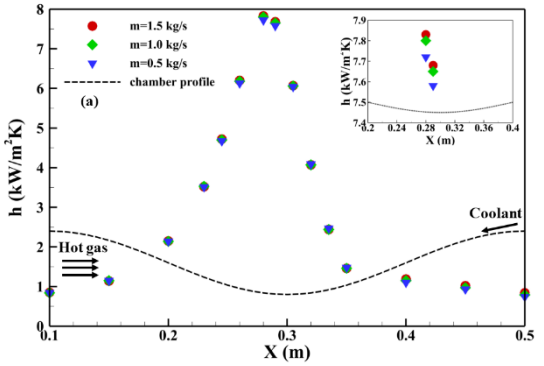

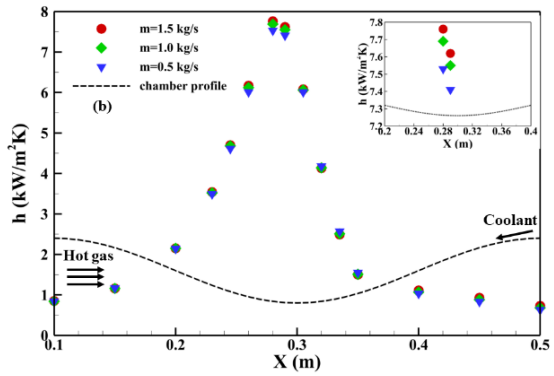

Fig. 10. Distribution of convective heat transfer coefficient: (a) water, (b) Ethyl-alcohol

Fig. 11 shows the Nusselt number variations versus Reynolds number for two coolants, water and Ethyl-alcohol, and different mass flow rate. The results indicate that as the coolant mass flow rate increases from 0.5 to 1.5 kg/s, the Reynolds and Nusselt number significantly increase. For mass flow rate of 1.5 kg/s, the ranges of Reynolds and Nusselt number are 1.8×10^5 to 6.1×10^5 and 802 to 2150 for water and 1.2×10^5 to 4×10^5 and 809 to 2168 for Ethyl-alcohol, respectively. Whereas, for mass flow rate of 0.5 kg/s, the ranges of Reynolds and Nusselt number are 0.6×10^5 to 2×10^5 and 333 to 891 for water and 0.3×10^5 to 1.3×10^5 and 336 to 900 for Ethyl-alcohol, respectively. This behavior confirms the changes in T_{wg}, T_{wc}, and convective heat transfer coefficient in terms of coolant mass flow rate.

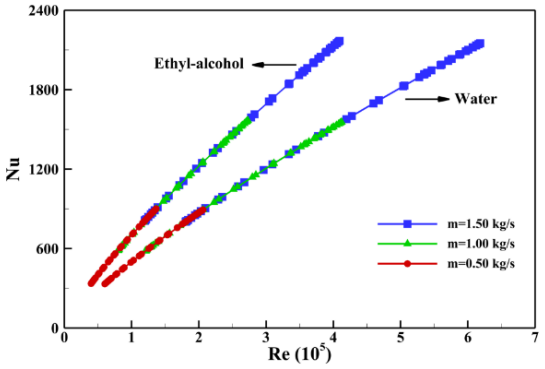

Fig. 11. Distribution of coolant Nusselt number versus Reynolds number

3.5. Distribution of Coolant Temperature

Fig. 12 depicts the distribution of T_{cool} along the thrust chamber for two coolants. As the coolant absorbs heat from the hot gas, its temperature progressively increases along the flow direction of the cooling channel. The slope of T_{cool} along the axial direction is approximately constant, except in a small region upstream of the throat (x=0.28) where the q is maximum, and in the sudden contraction region of the thrust chamber (x=0.12) where convective heat transfer increases significantly. Similar behavior of the T_{cool} has been observed in the investigation of [15, 18]. The critical point of water and Ethyl-alcohol is achieved at a temperature of 647 K and a pressure of 22 MPa, and at a temperature of 514 K and a pressure of 6 MPa, respectively. The maximum of T_{cool} for water and Ethyl-alcohol is 354 K and 372 K, respectively. In addition, the coolant pressure at the inlet of the cooling channel is considered to be sufficiently high such that, after accounting for the pressure drop along the channel, the outlet pressure reaches approximately 20 bar. Therefore, because the T_{cool} is lower than the critical temperature and the coolant pressure is higher than the critical pressure, the coolant will not reach the vapor state [36].

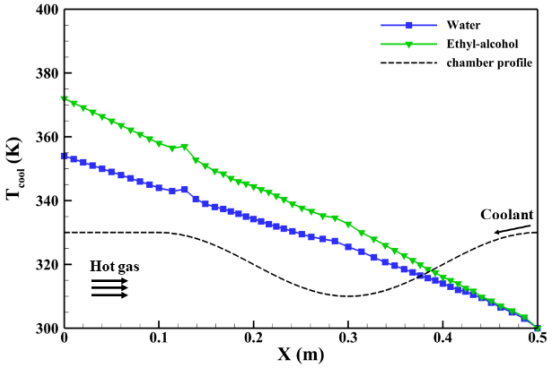

Fig. 12. Distribution of coolant temperature

4. Conclusions

In this study, the effect of coolants (water and Ethyl-alcohol) with different mass flow rates on the heat transfer characteristics of a regenerative cooling channel, such as T_{wg}, T_{wc}, T_{cool}, heat flux and convctive heat transfer coefficient has been explored for steady-state and transient conditions. For this purpose, a two-dimensional and axisymmetric model including the thrust chamber, cooling channel, and walls is used. According to the results of the study, the following conclusions can be drawn:

- Along the nozzle length, the temperature of the hot gas flow decreases from 3400 K to 2150 K, and the Mach number increases from 0.1 to 2.6.
- For both water and Ethyl-alcohol, the maximum T_{wg} occurs upstream of the throat (x=0.29), and throughout the thrust chamber, increasing the coolant mass flow rate significantly reduces the T_{wg}. The maximum T_{wg} at mass flow rate of 0.5 and 1.5 kg/s is calculated to be 657 and 541 Kelvin for water, and 957 and 693 Kelvin for Ethyl-alcohol, respectively.
- Throughout the thrust chamber, the T_{wc} is lower than the T_{wg}, with the maximum

difference between these two temperatures occurring upstream of the nozzle throat (x=0.29). In the upstream of the throat, the difference between the T_{wg} and the T_{wc} at mass flow rate of 0.5 and 1.5 kg/s has been calculated as 72 and 77 Kelvin for water, and 62 and 71 Kelvin for Ethyl-alcohol, respectively.

- From the start of engine operation, the wall temperature does not reach a steady state uniformly. Due to the coolant flow path in the cooling channel, the wall temperature of the nozzle divergent reaches a steady state first, followed by the throat and nozzle convergent, and finally, the wall temperature of the combustion chamber reaches a steady state over time. Increasing the coolant mass flow rate significantly reduces the time to reach a steady state of the T_{wg}. Thus, this time at mass flow rate of 0.5 and 0.1 kg/s is 5 and 2.5 seconds for water and 9 and 5 seconds for Ethyl-alcohol, respectively.
- The heat flux of gas-side flow decreases along the combustion chamber, increases along the converging nozzle, and decreases along the diverging nozzle, reaching its maximum value upstream of the throat (x=0.28). Variations in the coolant mass flow rate, except upstream of the throat, do not significantly affect the heat flux. The maximum heat flux at a mass flow rate of 1.5 kg/s is determined to be 21.0 and 19.7 for water and Ethyl-alcohol, respectively.
- The convective heat transfer coefficient is calculated using a direct approach and based on the T_{wg}, T_{bg}, and heat flux. The convctive heat transfer coefficient is maximum upstream of the throat (x=0.28). At this point, the coolant mass flow rate affects the heat transfer coefficient. In this way, increasing the coolant mass flow rate increases the convctive heat transfer coefficient of the wall.
- The T_{cool} continuously increases along the flow direction of the cooling channel with an almost constant slope.
- Overall, the results provide valuable guidance for the thermal design of regenerative cooling systems, particularly in balancing coolant mass flow rate, wall temperature reduction, and transient thermal response during engine start-up.

Nomenclature

C_p	Specific heat capacity [J/kg.K]
E	Energy [J]
h	Convective heat transfer coefficient [W/m^2.K]
H	Enthalpy [J/kg]
L	Length [m]
$\dot{m}$	Mass flow rate [kg/s]
P	Pressure [Pa]
Pr	Prandtl number
q	Heat flux [W/m^2]
r	Radius [m]
Re	Reynods number
t	Time [s]
t	Internal wall thickness [mm]
T	Temperature [K]
u	Velocity [m/s]
z	Cooling channel height [mm]

Greeks

ε	Expansion ratio
k	Turbulent kinetic energy [m^2/s^2]
λ	Thermal conductivity [W/m.K]
μ	Dynamic viscosity [kg/m.s]
ρ	Density [kg/m^3]
τ	Viscous shear stress [N/m^2]
ω	Specific dissipation rate [1/s]

Subscripts

in	Inlet
ex	Exit
ch	Chamber
no	Nozzle
wc	Wall cool
wg	Wall gas
bg	Bulk gas
cool	Coolant

Funding Statement

This research did not receive any specific grant from funding agencies in the public, commercial, or not-for-profit sectors.

Conflicts of Interest

The author declares that there is no conflict of interest regarding the publication of this article.

Authors Contribution Statement

Arash Haeri: Investigation, Data curation, Software.

Hamidreza Farshi Fasih: Project administration, Investigation, Writing-original draft.

Roohollah Rafee: Conceptualization, Methodology, Supervision.

References

[1] Jeon, T. J., Park, T. S., 2024. Thermal recycling analysis in regenerative cooling channels based on liquid rocket engine cycles. *Applied Thermal Engineering*, 256, 124095. https://doi.org/10.1016/j.applthermaleng.2024.124095

[2] Leonardi, M., Pizzarelli, M., Nasuti, F., 2018. A numerical procedure for the design of cooling channels for liquid rocket engines. *Space Propulsion Conference*, SP2018-00158.

[3] Pizzarelli, M., Carapellese, S., Nasuti, F., 2011. A quasi-2-D model for the prediction of the wall temperature of rocket engine cooling channels. *Numerical Heat Transfer A*, 60(1), pp. 1-24. http://dx.doi.org/10.1080/10407782.2011.578011

[4] Yang, W., Sun, B., 2013. Numerical simulation of liquid film and regenerative cooling in a liquid rocket. *Applied Thermal Engineering*, 54, pp. 460-469. http://dx.doi.org/10.1016/j.applthermaleng.2013.02.021

[5] Heldens, J. C., Fridh, J., Östlund, J., 2021. On the characterization of methane in rocket nozzle cooling channels. *Acta Astronautica*, 186, pp. 337–346. https://doi.org/10.1016/j.actaastro.2021.05.034

[6] Kim, S. K., Joh, M., Choi, S. H., Park, T. S., 2014. Effective modeling of conjugate heat transfer and hydraulics for the regenerative cooling design of kerosene rocket engines. *Numerical Heat Transfer A*, 66(8), pp. 863-883. http://dx.doi.org/10.1080/10407782.2014.892396

[7] Shanmugam, A. R., Park, K. S., 2024. Flow and heat transfer of supercritical hydrogen in a regenerative cooling channel with the arc ribs of a rocket engine. *Applied Thermal Engineering*, 236, 121451. https://doi.org/10.1016/j.applthermaleng.2023.121451

[8] Nasser, I., Haidn, O., Manfletti, C., 2023. Numerical investigation of rocket engine cooling channel heat transfer for different LNG under trans-critical conditions. *International Journal of Thermofluids*, 20, 100461. https://doi.org/10.1016/j.ijft.2023.100461

[9] Engblom, W., Fletcher, B., Georgiadis, N., 2008. Conjugate Conduction-Convection Heat Transfer for Water-Cooled High-Speed Flows. *AIAA*, 2008-4653. https://doi.org/10.2514/6.2008-4653

[10] Zhao, J., Li, S., Zhang, X., Sun, M., Song, Y., 2023. Enhanced heat transfer of supercritical *n*-decane in cooling channels with triangular ribs for regenerative cooling. *Applied Thermal Engineering*, 218, 119369. https://doi.org/10.1016/j.applthermaleng.2022.119369

[11] Wang, L., Chen, Z., Meng, H., 2013. Numerical study of conjugate heat transfer of cryogenic methane in rectangular engine cooling channels at supercritical pressures. *Applied Thermal Engineering*, 54, pp. 237-246. http://dx.doi.org/10.1016/j.applthermaleng.2013.02.007

[12] Zhang, X., Guo, W., Gao, G., Xi, W., Liu, J., Sunden, B., 2025. Numerical investigations of flow and heat transfer characteristics of a regenerative cooling channel using supercritical CO_2 with different cross-section shapes. *International Journal of Thermal Sciences,* 215, 109965. https://doi.org/10.1016/j.ijthermalsci.2025.109965

[13] Buchholz, M., Gruber, S., Selbmann, A., Marquardt, A., Meier, L., Müller, M., Seifert, L., Leyens, C., Tajmar, M., Bach, C., 2023. Flow rate improvements in additively manufactured flow channels suitable for rocket engine application. *CEAS Space Journal*, 15, pp. 715-728. https://doi.org/10.1007/s12567-022-00476-7

[14] Zhou, C., Yu, N., Wang, S., Han, S., Gong, H., Cai, G., Wang, J., 2023. The influence of thrust chamber structure parameters on regenerative cooling effect with hydrogen peroxide as coolant in liquid rocket engines. *Aerospace*, 10, 65. https://doi.org/10.3390/aerospace10010065

[15] Junjie, L., Guanquan, D., Ping, J., Ruizhi, L., 2023. Heat transfer analysis and structural optimization for spiral channel regenerative cooling thrust chamber. *International Journal of Aerospace Engineering*, 8628107. https://doi.org/10.1155/2023/8628107

[16] Zhang, Q., Xue, T., Zhang, X., 2024. Advancing heat transfer efficiency: V-shape crossed structures in regenerative cooling channels for rocket engines. *International Communications in Heat and Mass Transfer,* 158, 107921. https://doi.org/10.1016/j.icheatmasstransfer.2024.107921

[17] Marchi, C. H., Laroca, F., Silva, A. F. C., Hinckel, J. N., 2004. Numerical solutions of flow in rocket engines with regenerative cooling. *Numerical Heat Transfer A*, 45, pp. 699-717. https://doi.org/10.1080/10407780490424307

[18] Song, J., Sun, B., 2016. Coupled numerical simulation of combustion and regenerative cooling in LOX/Methane rocket engines.

Applied Thermal Engineering, 106, pp. 762-773. http://dx.doi.org/10.1016/j.applthermaleng.2016.05.130

[19] Shokri, M., Ebrahimi, A., 2018. Heat transfer aspects of regenerative-cooling in methane-based propulsion systems. *Aerospace Science and Technology*, 82, pp. 412-424. https://doi.org/10.1016/j.ast.2018.09.025

[20] Farshi Fasih, H., Ghassemi, H., Karimi Mazraeshahi, H., 2022. Numerical investigation on gasification process of heavy fuel oil in an entrained flow gasifier. *Petroleum Science and Technology*, 41, pp. 524-545. https://doi.org/10.1080/10916466.2022.2062383

[21] Song, J., Liang, T., Li, Q., Cheng, P., Zhang, D., Cui, P., Sun, J., 2021. Study on the heat transfer characteristics of regenerative cooling for LOX/LCH_4 variable thrust rocket engine. *Case Studies in Thermal Engineering*, 28, 101664. https://doi.org/10.1016/j.csite.2021.101664

[22] Song, J., Cui, P., Li, Q., Cheng, P., Chen, L., Liang, T., 2022. System scheme and thermal performance of a third fluid cooled rocket engine. *Acta Astronautica*, 191, pp. 204-215. https://doi.org/10.1016/j.actaastro.2021.11.004

[23] Liu, S., Cheng, Q., Han, L., Zhang, W., Wang, G., Li, Y., 2024. The influence of asymmetric truncated ribs on flow and heat transfer of supercritical aviation kerosene in a rectangular curved cooling channel. *International Journal of Thermal Sciences*, 196, 108720. https://doi.org/10.1016/j.ijthermalsci.2023.108720

[24] Kostić, O. P., Stefanović, Z. A., Kostić, I. A., 2015. CFD modeling of supersonic airflow generated by 2D nozzle with and without an obstacle at the exit section. *FME Transactions*, 43, pp. 107-113. DOI:10.5937/FMET1502107K

[25] Yan, Z., Chen, Y., Wu, Y., Liu, Z., Gao, Y., Wang, W., 2023. A system-level multi-field coupling algorithm for regenerative cooling thrust chamber of a LOX/methane rocket engine. *Acta Astronautica*, 213, pp. 588-602. https://doi.org/10.1016/j.actaastro.2023.09.042

[26] Kim, S. K., Joh, M., Choi, H. S., Park, T. S., 2014. Multidisciplinary simulation of a regeneratively cooled thrust chamber of liquid rocket engine: turbulent combustion and nozzle flow. *International Journal of Heat and Mass Transfer,* 70, pp. 1066-1077. http://dx.doi.org/10.1016/j.ijheatmasstransfer.2013.10.046

[27] Kang, Y. D., Sun, B., 2011. Numerical Simulation of Liquid Rocket Engine Thrust Chamber Regenerative Cooling. *Journal of Thermophysics and Heat Transfer*, 25, pp. 155-164. https://doi.org/10.2514/1.47701

[28] Ulas, A., Boysan, E., 2013. Numerical analysis of regenerative cooling in liquid propellant rocket engines. *Aerospace Science and Technology*, 24, pp. 187-197. https://doi.org/10.1016/j.ast.2011.11.006

[29] Gallo, G., Kamps, L., Hirai, S., Carmicino, C., Nagata, H., 2023. One-dimensional modelling of the nozzle cooling with cryogenic oxygen flowing through helical channels in a hybrid rocket. *Acta Astronautica*, 210, pp. 176-196. https://doi.org/10.1016/j.actaastro.2023.05.013

[30] Rajagopal, M., 2015. Numerical modeling of regenerative cooling system for large expansion ratio rocket engines. *Journal of Thermal Science and Engineering Applications*, 7, 011012. https://doi.org/10.1115/1.4028979

[31] Negishi, H., Daimon, Y., Negoro, N., Kurosu, A., 2015. Regenerative cooling performance analysis of the LE-X engine combustion chamber. *AIAA*, 2015-3760. https://doi.org/10.2514/6.2015-3760

[32] Eiringhaus, D., Riedmann, H., Knab, O., Haidn, O. J., 2019. 3D Conjugate heat transfer analysis of a 100 kN class liquid rocket combustion chamber. *8TH European conference for aeronautics and aerospace sciences.* DOI: 10.13009/EUCASS2019-251

[33] Daimon, Y., Negishi, H., Kawashima, H., 2019. Conjugated combustion and heat transfer simulations of upper and lower main combustion chambers of LE-9 engine. *AIAA*, 2019-4112. https://doi.org/10.2514/6.2019-4112

[34] Naraghi, M.H., Dunn, S., Coats, D., 2004. A model for design and analysis of regeneratively cooled rocket engines. *AIAA*, 2004-3852. https://doi.org/10.2514/6.2004-3852

[35] Pu, H., Li, S., Dong, M., Jiao, S., Shang, Y., 2018. Numerical method for coupled thermal analysis of the regenerative cooling structure. *Journal of Thermophysics and Heat Transfer*, 23. https://doi.org/10.2514/1.T5224

[36] Fouladi, N., Farahani, M., Dowlatabadi, M. M., 2025. Cooling system design and analysis for high heat flux large dimension diffuser of a high-altitude test facility. *International Journal of Thermofluids*, 25, 101030. https://doi.org/10.1016/j.ijft.2024.101030